Heliyon 9 (2023) e18582

Contents lists available at ScienceDirect

Heliyon

journal homepage: www.cell.com/heliyon

Comparative evaluation and sensitivity analysis of multi-modelling and optimization of milling Ti–6Al–4V alloy with high-pressure coolant jets

Mst Nazma Sultana [a,*], Nikhil Ranjan Dhar [b]

[a] Department of Industrial Engineering and Management, Khulna University of Engineering & Technology, Khulna-9203, Bangladesh
[b] Department of Industrial and Production Engineering, Bangladesh University of Engineering & Technology, Dhaka-1000, Bangladesh

ARTICLE INFO

Keywords:
Modelling
Response surface methodology
Artificial neural network
Adaptive neuro fizzy inference system
Multiple-objective optimization on the basis of ratio analysis
Sensitivity analysis

ABSTRACT

An effective cooling method with the proper selection of process parameters can intensify the machining performance by reducing the loss of resources with better quality products. In this regard, modelling is an appropriate way of predicting responses in changing environment and optimization is an efficient tool of selecting the best process parameters based on the specific desire. With a view to enhance the machinability of Ti–6Al–4V alloy, the first attempt of the current study was to predict the performance characteristics of milling such as cutting force (N), specific cutting energy (J/mm^3) and surface roughness (μm) with the variation of speed (m/min), feed (mm/min), depth of cut (mm) and cooling approach by developing mathematical models. For the present work, three different predictive models such as response surface methodology (RSM), artificial neural network (ANN), and adaptive neuro fuzzy inference system (ANFIS) was followed. Additionally, a comparative assessment of the used predictive models was carried out and ANFIS was noticed as the most accurate predictive model. After that, optimization of the selected responses was conducted by multiple-objective optimization on the basis of ratio analysis (MOORA) method where the relative weights of each response were defined by principal component analysis (PCA). For milling Ti–6Al–4V alloy within the specific boundary conditions, PCA-MOORA suggested an optimal parameter setting at 32 m/min speed, 22 mm/min feed rate, and 0.75 mm depth of cut with rotary high-pressure cooling. Finally, the sensitivity of the used MOORA method with the variation of unitary ratio was checked out to take a robust decision.

1. Introduction

Milling is a complex intermittent cutting process that is extensively used in producing flat plain surfaces of both simple and intricate parts by using a multi-point cutter. Many studies have already explored the various aspects of machinability of Ti–6Al–4V alloy in dry milling such as cutting temperature, cutting forces, power consumption, surface roughness, and tool wear [1–4]. Exploring the abovementioned studies, it has been discovered that the excess heat generation with drastic tool wear, higher surface roughness, frequent tool vibrations, and higher cutting forces hinder dry milling of Ti–6Al–4V alloy. Currently, researchers have focused on effective cooling approaches such as minimum quantity lubrication (MQL), high-pressure cooling (HPC), and cryogenic cooling.

* Corresponding author.
E-mail address: nazma.kuet@yahoo.com (M.N. Sultana).

https://doi.org/10.1016/j.heliyon.2023.e18582
Received 29 April 2023; Received in revised form 21 June 2023; Accepted 21 July 2023
Available online 22 July 2023

Among those, HPC is regarded as one of the prominent cooling technologies for efficiently managing cutting temperature as well as lubricating surfaces. High-pressure coolant jets significantly reduce abrasion, microcracks, and chipping, hence preventing premature tool failure [5]. Furthermore, HPC boosts productivity by minimizing residual stress and giving a superior surface quality with appropriate chip removal at a faster rate. However, in respect of proper cooling/lubrication in milling, two issues are needed to resolve-cooling the complex helix-shaped rotating cutter and successfully lubricating the interface between tool-work. Some studies suggested internal cooling to overcome these issues [6]. However, the fundamental disadvantage of this internal cooling is that it has a drastic impact on tool strength [7]. As a result, a difference in the cooling approach is to be expected. To fill this void, an external rotary liquid applicator for providing high-pressure coolant jets was conceptualized and fabricated. The performance of the developed applicator was evaluated in terms of cutting force, specific cutting energy, and surface roughness.

The emerging application areas of Ti–6Al–4V alloy (automotive, aerospace components) necessitate highly precise machined parts since the functionality of machined parts is dependent on the degree of surface finish, which is just opposite to surface roughness. Surface finish qualitatively denotes surface evenness without cracks, holes, or other imperfections, whereas surface roughness quantitatively shows surface irregularities. Because of its quantitative nature and straightforward calibration procedure, average surface roughness is often used as a measure of surface integrity. Cutting force is another notable measure of performance because it represents the machining status [8]. In addition, excessive tool wear with higher cutting force degrades the surface quality. To achieve a cost-effective machining process, reduction of power consumption is necessary that is directly linked with specific cutting energy. In a nutshell, it can be claimed that it is imperative to find out the effects of process parameters on those responses for attaining the desired machinability in milling Ti-alloy.

Soft Computing (SC) imitates the human brain by utilizing soft values and fuzzy sets, as well as the ability to operate in an uncertain environment. This feature broadens its application in the manufacturing industry for anticipating and modelling behaviours. Common SC technologies include regression analysis, Taguchi method (TM), response surface methodology (RSM), artificial neural network (ANN), fuzzy logic (FL), adaptive neuro-fuzzy inference systems (ANFIS), sintered annealing (SA), data envelopment analysis (DEA), and support vector machines (SVM) [9]. Among the mentioned SC technologies, RSM, ANN, and ANFIS were chosen as prediction models in this study with fewer resources and time. RSM is a powerful statistical tool with fewer experimental runs than full factorial-based design of experiment (DoE), used in different machining processes by researchers [10]. Shetty et al. [11] studied the minimum quantity lubrication (MQL) turning of Ti–6Al–4V alloy in terms of speed, feed, and depth of cut using RSM. Hashmi et al. [12] conducted high-speed milling of Ti–6Al–4V alloy without coolant and concluded that surface roughness is mostly governed by the depth of cut, whereas cutting velocity and feed rate have no major effects based on the analysis of RSM. Daramola et al. [2] used RSM to explore the influence of milling process parameters on resulting forces and found that RSM is a useful numerical technique for creating realistic DOE models that properly anticipate machining responses. Another effective prediction approach in anticipating machining outcomes with process parameter variations is ANN. Because of its strong generalization strength, numerous researchers have already used this AI approach in diverse applications. Zain et al. [13] applied ANN by changing the number of layers and functions for predicting roughness accurately in milling and suggested that high speed with a low feed rate and radial rake angle produces the optimum surface roughness value. Namlu et al. [14] reported that ANN can predict surface roughness in milling Ti–6Al–4V alloy with a mean absolute percentage error (MAPE) of 1.85%. ANFIS has recently been proven to be another effective prediction tool in engineering applications by several researchers. Al-Zubaidi et al. [15] investigated the ANFIS model's predictability in anticipating surface roughness in milling Ti–6Al–4V alloy and found a minimal root mean square error (RMSE) of 0.1030. The predictability of the ANFIS model changes with membership functions. Bandapalli et al. [16] discovered that the gbell membership function had the lowest prediction error (0.04%) when compared to triangular and trapezoidal membership functions. It is critical to assess the prediction models to choose the most suited one. With this in mind, researchers are now driven to conduct a comparative examination of many widely used models in specific issues. Manufacturers will be able to determine the most appropriate approach capable of generating a quick and precise performance by employing an accurate modelling technique for the design of an efficient machining process. Klickcap et al. [17] developed ANN and RSM models for predicting cutting force and surface roughness in dry milling of Ti alloy but no clear comparative analysis in selecting the best predictive model was explained. Karkalos et al. [4] investigated surface roughness in milling Ti–6Al–4V alloy using both the statistical RSM model and ANN model. The authors concluded that in terms of roughness prediction, the ANN model outperforms RSM, whereas RSM is better for optimizing process parameters. The better predictability of ANN over RSM was also divulged by another research work conducted by Yanis et al. [18]. Sada and Ikpeseni [19] compared the predictability of ANN and ANFIS in projecting tool wear and surface roughness in turning medium carbon steel, concluding that ANN is more predictable than ANFIS. Gupta et al. [20] compared RSM with ANFIS in assessing the performance of several nanofluids in turning Ti–6Al–4V alloy and found that ANFIS outperformed RSM. Onu et al. [21] researched on estimating the fraction adsorption of EBT using RSM, ANN, and ANFIS, with a critical evaluation of the three models' prediction powers, noting that ANFIS is superior to the other two. But, no comparative study on the performance evaluation of RSM, ANN, and ANFIS in milling Ti–6Al–4V alloy with high pressure cooling was found that motives us to do this job.

The optimization model, in addition to the prediction models, is required to construct an optimal design matrix for better output. There are a variety of advanced evolutionary optimization strategies to choose from. Many researchers in the engineering and industrial areas use the MOORA method, which is a simple and well-known optimization strategy [22]. To optimize surface roughness and kerf taper angle of composites in abrasive water jet machining, MOORA method was used by Kalirasu et al. [23]. Khan and Maity [24] recommended MOORA as a robust and time-saving optimization method. Not only in machining but also in some other applications such as for material selection problems, MOORA was proposed by researchers [25]. To increase the accuracy of the MOORA method, some researchers proposed PCA as an extended tool for determining the relative weights of each criterion in any specific case. Majumder and Maity [26] suggested PCA based MOORA as an efficient way of optimization in WEDM of titanium alloy. Zaman et al.

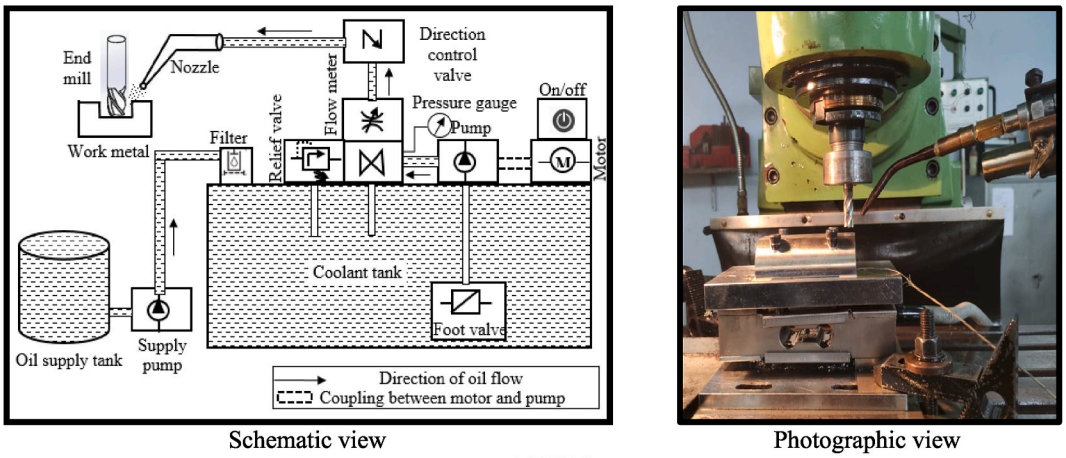

Fig. 1. Experimental set up.

[27] used PCA-MOORA in turning 42CrMo4 and suggested the optimal parameter settings as speed of 352 m/min and feed of 0.10 mm/rev under MQL. In recent manufacturing applications, sensitivity analysis is crucial to test the robustness of the used optimization model. Very few researchers have assessed the model's sensitivity systematically. Li et al. [28] conducted a sensitivity analysis of the TOPSIS method with equal criteria weights in determining water quality. Following that, Bhadra et al. [29] performed sensitivity

analysis of the criteria importance through inter-criteria correlation (CRITIC) and Analytic Hierarchy Process (AHP) for order of preference by similarity to ideal solution (TOPSIS) methods to select the best natural fiber for aerospace cabin interior. In this study, it is tried to perform sensitivity analysis of the MOORA method considering the different relative weight of criterion derived by PCA.

As referred to previous studies, it is clear that a lot of research works have already been carried out in optimizing process parameters and modelling milling responses but no research study concerning the sensitivity analysis of the used optimization model with the variation of the unitary ratios of selected responses was noticed. To bridge that gap, this paper attempts to perform sensitivity analysis of the used MOORA method along with the prediction and modelling of the cutting force, specific cutting energy, and surface roughness in milling by using RSM, ANN, and ANFIS. Moreover, the developed models were comparatively assessed based on different statistical error analysis.

2. Methodology

2.1. Machining methods

The work material, Ti–6Al–4V alloy (Grade 5), had an average hardness of around 37 HRC was chosen for its versatility. The chemical composition of the used alloy is: 6.41% Al, 4.44% V, 0.40% Fe, 1.19% O, 4.13% C and 83.71% Ti. Four flute high-speed steel (HSS) end mill cutter (Dormer, ENGLAND) with 0º rake angle, 15° clearance angle, 30º uniform helix angle, and 65 HRC hardness was employed for slot milling. The thermophysical properties of the cutting tool can be specified as follows: density 7600 kg/m^3, Young's modulus 233 GPa, Poisson's ratio 0.30, specific heat 461 J/kg-^{0}C, thermal conductivity 20.2 W/m-^{0}C [30]. During milling, the cutter was rigorously supported and rotated vertically by collet with jam nut. Using a vertical milling machine (Sunlike, China, power: 7hp), experimental tests were carried out under three different cutting environments: dry, high-pressure cooling (HPC), and rotary high-pressure cooling (RHPC). This research used speed (V_c) of 16~32 m/min, table feed rates (f) of 22~68 mm/min, and cutting depths (a_p) of 0.5–1.0 mm. VG-68 (viscosity grade 68) was chosen as the high-pressure coolant for both HPC and RHPC that boosts oxidation resistance and metal passivation. The specific characteristics of the used cutting fluid were: density 932 kg/m^3 at 20 °C, viscosity index 68 at 40 °C, and flash point at 300° [31]. Fig. 1 depicts the experimental setups for HPC and RHPC aided end milling of Ti–6Al–4V alloy. In the designed applicator (as shown in Fig. 1(c)), cutting fluids were passed through the oil chamber (kept stationary) to the adapter (rotary) which is supported by a spindle with a jam nut. Next, oil enters into a secondary mini oil chamber which was attached and rotated with the adapter and embedded with four nozzles (dia. 0.50 mm) for supplying high-pressure coolant jets. The end mill cutter was supported by a collet and specially designed jam nut. So, the angular velocity of the cutter and rotary chamber was same.

In this study, cutting force (F_c) was measured by using a KISTLER dynamometer equipped with a load cell and charge amplifier during milling. After that, specific cutting energy (SCE) was calculated mathematically by using the following Eqn. (1):

$$SCE = \frac{F_c}{f \times a_p}, \frac{J}{mm^3}; \tag{1}$$

Rank Hobson's Surtronic 3+ portable roughness checker (with a sampling length of 0.8 mm) was used to measure mean surface roughness (R_a) after each experimental trial run. The experiments were designed by following the Box Behnken Design (BBD) approach of RSM. For the current study, response surface methodology (RSM) was selected as the statistical prediction model, artificial neural network (ANN) and adaptive neuro fuzzy inference system (ANFIS) were employed as artificial intelligence approaches.

2.2. Response surface methodology (RSM)

The first step in determining the appropriate process parameters is to generate mathematical models of the process to establish a link between the process's inputs and outputs. RSM is a popular statistical approach for establishing a specific relationship between a set of influential input factors and a set of performance indicators [32]. Based on previous research conducted by Zaman and Dhar [33], BBD based RSM models were employed in this work to show the mathematical relationships between the specified responses (cutting force, specific cutting energy, and surface roughness) and a set of independent factors (speed, feed, depth of cut, and cooling approaches). In general, a first-order polynomial is appropriate for determining the main effects of individual input variables and for a relatively small region of the independent variable space (low response curvature), whereas a second-order model can be used to determine the interaction effects of variables on output quality (Mia et al., 2017). Mathematical expressions for both first-order and second-order models can be written symbolically as in Eqns. (2) and (3), respectively.

$$y = \alpha_0 + \alpha_1 x_1 + \alpha_2 x_2 + \ldots + \alpha_n x_n; \tag{2}$$

$$y = \alpha_0 + \alpha_1 x_1 + \sum_{i=1}^{n} \alpha_i x_i + \sum_{i=1}^{n} \alpha_{ii} x_i^2 + \sum_{i,j}^{n} \alpha_{ij} x_i x_j + \in; \tag{3}$$

The regression coefficients of the linear, quadratic, and interaction terms are represented by the variables α_0, α_i, α_{ii} and α_{ij}, respectively. The input variables relating to speed (V_c), feed rate (f), and depth of cut (a_p) are represented by x_i . Since the input variable cooling approach (CA) is a categorical variable, three different forms of Eqns. were produced for dry, HPC, and RHPC. Additionally, analysis of variance (ANOVA) was employed to demonstrate the effects of each factor and their interactions on the

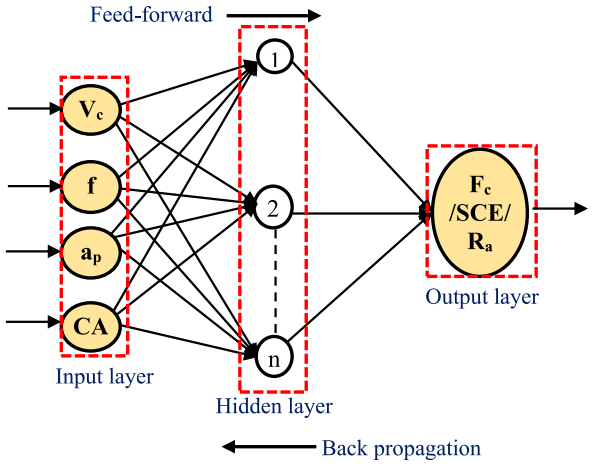

Fig. 2. 4-*n*-1 multi-layer ANN structure.

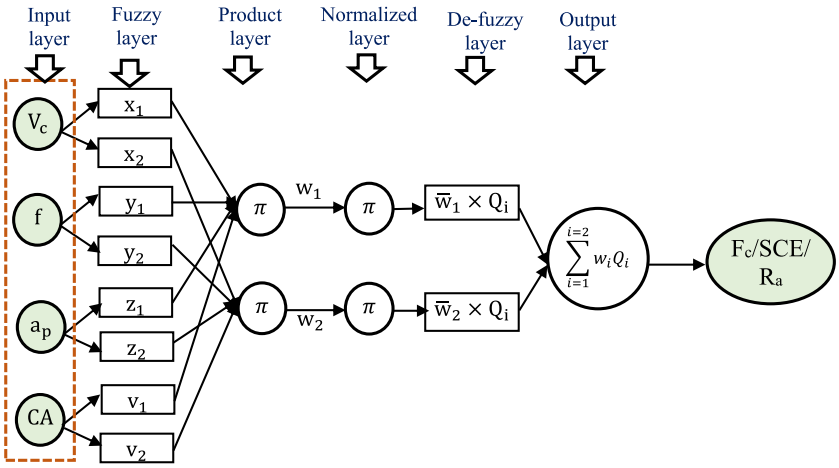

Fig. 3. Proposed five-layered ANFIS structure with two rules.

responses [34]. A random experimental error is represented by the symbol ∈.

2.3. Artificial neural network (ANN)

A non-linear, multi-layered (input layer, hidden layer, and output layer) prediction system called an artificial neural network (ANN) can model complex issues just like the human brain [35]. Each layer is made up of one or more neurons. While, the input layer contains input variables as neurons, the output layer comprises a single neuron for each output variable. Trial and errors are needed to determine the number of layers and neurons in the hidden layer, which influences the accuracy and predictability of the adopted ANN model. Due to the higher complexity of multiple hidden layers, one hidden layer was used in this study to form the network [36]. Using the 'nntool' wizard of MATLAB 2019, a 4-*n*-1 multi-layer feed-forward backpropagation (FFBPN) type network was created (as shown in Fig. 2), where 'n' is the number of neurons in hidden layer. The number of neurons for the hidden layer was varied within 3∼39. Because of its superior ability to handle less random training data sets without a cross-validation test and less noise, the Bayesian Regularization (TrainBR) algorithm was chosen for the training network [37]. The learning function was used as gradient descent with momentum weight and bias (LEARNGDM) [38]. Finally, 'TANSIG' for the hidden layer and 'PURELIN' for the output layer were used [39]. The Absolute percentage error (APE), mean absolute percentage error (MAPE), and coefficient of determination (R^2) were used to assess the effectiveness of the networks that were created.

2.4. Adaptive neuro-fuzzy inference system (ANFIS)

ANFIS is another widely used hybrid AI approach for accurate prediction and modelling of complicated nonlinear issues, comprised

of fuzzy logic theory and a self-learned adaptive ANN approach [35]. Fuzzy logic contains a set of theoretical linguistics if-then rules that can approximate thinking in any real-world scenario [40]. However, due to a lack of learning ability, it is unable to adapt to uncertain environments [41]. ANN, on the other hand, can deal with ambiguous situations by training raw data acquired from any external source but unable to explain [20]. In ANFIS, the benefits of fuzzy logic if-then rules are blended with ANN to create a hybrid neuro-adaptive intelligence system. The ANFIS structure is comprised of five layers: the fuzzy layer, the product layer, the normalized layer, the de-fuzzy layer, and the output layer. The Fuzzy layer converts the received inputs from the outer sources into fuzzy sets using various membership functions (MFs) and this layer contains adaptive nodes with multiple rules. Next, the product layer calculates the firing strength of the received fuzzy inputs from the previous layer. After that, the normalization layer converts firing strength into unitless values which are transformed into crisp values in the De fuzzy layer. The cumulative sum of the de-fuzzy layer's obtained outputs is computed based on 'wtaver' command and signified by a fixed node. The suggested ANFIS model for the current study was designed in MATLAB R2019a using a fuzzy toolbox to analyze the link between inputs (V_c, f, a_p, and CA) and outputs such as cutting force (F_c), specific cutting energy (SCE), and surface roughness (R_a). The structure of the proposed ANFIS model is drawn in Fig. 3.

2.5. Integrated PCA-MOORA method

Principal component analysis (PCA) was first proposed by Pearson [42] and then, explored by Hotelling [43] to evaluate the weights of different quantitative objectives. This statistical weight evaluation method transformed correlated variables into linear non-correlated variables which are defined as principal components. Initially, a decision matrix of responses for all alternatives was formed as seen in Eqn. (4):

$$X = \begin{bmatrix} x_{11} & x_{12} & \dots & \dots & x_{1n} \\ x_{21} & x_{22} & \dots & \dots & x_{2n} \\ \dots & \dots & \dots & \dots & \dots \\ x_{m1} & x_{m2} & \dots & \dots & x_{mn} \end{bmatrix}; \tag{4}$$

Where, x_{ij} is the measured response of ith alternative on jth objective, m corresponds to the number of experimental observations = 39, and n represents the number of responses = 3. Then the correlation coefficient was calculated by using the following Eqn. (5):

$$r_{jz} = \frac{\mathrm{cov}(x_i(j), x_i(z))}{\sigma_{x_i}(j) \times \sigma_{x_i}(z)};\ \begin{matrix} y = 1, 2, \dots\dots\dots, n \\ z = 1, 2, \dots\dots\dots, n. \end{matrix} \tag{5}$$

Where, $\mathrm{cov}(x_i(j), x_i(z))$ symbolizes the covariance of $x_i(j)$ and $x_i(z)$ sequence, $\sigma_{x_i(j)}$ and $\sigma_{x_i(z)}$ are the standard deviations of $x_i(j)$ and $x_i(z)$, respectively. Finally, the principal components were estimated by using Eqn. (6) and then, arranged in descending order based on variability. The data obtained by the first principal component with the maximum variability were used to establish the relative weights of objectives.

$$P_{mk} = \sum_{i=1}^{n} x_m(i) \times E_{ik}\ ;\ P_{mk}, \text{the first principal component and } E_{ik}, \text{the eigen vector.} \tag{6}$$

The Eigen vector (E_{ik}) can be mathematically determined by using the correlation coefficient value r_{yz} as presented inEqn. (7):

$$E_{ik}(r - \lambda_k I_m) = 0\ ;\ \lambda_k \text{ denotes the Eigen value.} \tag{7}$$

The MOORA method is recommended by many researchers in decision making because it assists in selecting the best option from a large number of candidate alternatives for a particular situation. This approach was introduced by Brauers and Zavadskas [44]. The first stage of this method is to create a decision matrix that displays the performance of numerous alternatives in terms of various quantitative objectives as presented in Eqn. (4). After that, the normalized and weighted normalized decision matrix are required to form by using Eqns. (8) and (9), respectively, where weights 'w_j' for each j objective can be derived by using PCA.

$$N_{ij} = \frac{x_{ij}}{\sqrt{\sum_{j=1}^{3} x_{ij}^2}}; \tag{8}$$

$$WN_{ij} = w_j \times N_{ij}; \tag{9}$$

Finally, the computation of the weighted overall assessment value X_i* can be conducted by adding up the performance measures for all the maximizing criteria and subtracting the similar for the minimizing criteria by using Eqn. (10).

$$X_i^* = \sum_{j=1}^{b} WN_{ij} - \sum_{j=b+1}^{n} WN_{ij}; \tag{10}$$

Where, b is the number of objectives to be maximized, (*n*-b) denotes the number of objectives to be minimized, and X_i^* represents the normalized weighted assessment value of the ith alternative in relation to all the objectives.

Table 1
BBD design matrix of input variables with their corresponding responses.

Experimental alternatives	Speed (V_c), m/min	Feed rate (f), mm/min	Depth of cut (a_p), mm	Cooling approach (CA)	Cutting force (F_c), N	Specific cutting energy (SCE), J/mm^3	Surface roughness (R_a), μm
1	24	45	0.75	3	292	8.65	0.84
2	32	22	0.75	2	216	13.09	0.78
3	24	68	1.00	3	378	5.56	1.32
4	16	68	0.75	2	426	8.35	1.52
5	24	68	0.50	3	298	8.76	1.18
6	24	45	0.75	2	301	8.92	1.24
7	24	68	1.00	2	416	6.12	1.59
8	32	22	0.75	3	202	12.24	0.64
9	16	45	1.00	1	481	10.69	1.63
10	32	22	0.75	1	280	16.97	1.18
11	32	45	1.00	1	377	8.38	1.32
12	24	68	0.50	1	419	12.32	1.74
13	24	45	0.75	1	342	10.13	1.41
14	24	22	1.00	3	314	14.27	0.96
15	32	68	0.75	2	328	6.43	1.02
16	16	68	0.75	3	387	7.59	1.50
17	16	22	0.75	3	289	17.52	1.10
18	32	45	0.50	3	213	9.47	0.74
19	24	22	1.00	1	384	17.45	1.47
20	16	22	0.75	2	333	20.18	1.22
21	16	45	0.50	3	283	12.58	0.98
22	32	45	1.00	3	308	6.84	1.00
23	24	22	0.50	3	189	17.18	0.72
24	24	68	1.00	1	458	6.74	2.25
25	32	68	0.75	1	351	6.88	1.68
26	32	45	0.50	1	289	12.84	1.35
27	24	22	0.50	2	213	19.36	0.88
28	16	45	1.00	2	435	9.67	1.44
29	32	45	1.00	2	333	7.40	1.24
30	16	45	1.00	3	377	8.38	1.30
31	16	68	0.75	1	473	9.27	2.15
32	32	45	0.50	2	270	12.00	0.84
33	24	22	0.50	1	243	22.09	1.53
34	16	45	0.50	2	316	14.04	1.14
35	24	22	1.00	2	335	15.23	1.34
36	24	68	0.50	2	368	10.82	1.24
37	16	45	0.50	1	363	16.13	1.58
38	16	22	0.75	1	362	21.94	1.39
39	32	68	0.75	3	302	5.92	1.00

2.6. Sensitivity analysis

Different statistical error functions, such as APE, and MAPE (as expressed in mathematical form in Eqns. (11) and (12), respectively) were used to examine the predictive power of the RSM, ANN, and ANFIS.

$$\mathrm{APE} = \frac{|\text{actual} - \text{predicted}|}{\text{actual}} \times 100\%; \tag{11}$$

$$\mathrm{MAPE} = \frac{\frac{|\text{actual}-\text{predicted}|}{\text{actual}} \times 100\%}{\text{no. of trial runs}}; \tag{12}$$

The stability of ranking alternatives by MOORA method was checked out by performing sensitivity analysis. For this, the relative weights of the selected responses were altered. The systematic way of sensitivity analysis can be briefly described as follows [28]:

Step 1: To impose any disturbance weight $w_k^{'}$ instead of initial weight w_k. The mathematical relation between w_k and $w_k^{'}$ can be expressed as in the form of Eqn. (13):

$$\gamma_k = \frac{w_k^{'}}{w_k}\ ;\ \text{where } \gamma_k \text{ symbolizes the unitary ratio and } k = 1, 2, \ldots\ldots, n. \tag{13}$$

Step 2: To calculate the changed weights of other responses $w_n^{'}$ in respect to $w_k^{'}$ considering the sum of all weights equal to 1, the following Eqn. (14) may be used:

$$w_n^{'} = \frac{w_n}{1 + (\beta_k - 1)w_k}\ ;\ \text{where } \beta_k = \frac{\gamma_k - \gamma_k\delta_k}{1 - \gamma_k\delta_k} \text{ represents the initial variation ratio.} \tag{14}$$

Table 2
ANOVA results of cutting force (F_c).

Response	Source	SS	DF	MS	F-value	p-value	PC
	V_c	46,464	1	46,464	263	<0.0001	21.81
	F	64,480	1	64,480	365	<0.0001	30.27
	a_p	53,392	1	53,392	302	<0.0001	25.06
	CA	37,766	2	18,883	107	<0.0001	17.73
	$V_c \times a_p$	602	1	602	3.41	0.0746	0.28
	$f \times a_p$	4070	1	4070	23.07	<0.0001	1.91
	a_p^2	967	1	967	5.48	<0.0001	0.45
	$\in$	5293	30	176.4			2.48
	Total	213,034	38				100.00

Table 3
ANOVA results of specific cutting energy (SCE).

Response	Source	SS	DF	MS	F-value	p-value	PC
	V_c	59.75	1	59.75	166.82	<0.0001	7.12
	F	529.74	1	529.74	1478.95	<0.0001	63.33
	a_p	107.92	1	107.92	301.29	<0.0001	12.64
	CA	52.49	2	26.24	73.27	<0.0001	6.31
	$V_c \times f$	10.74	1	10.74	29.99	<0.0001	1.29
	$f \times CA$	6.47	2	3.23	9.03	0.0011	0.78
	$a_p \times CA$	3.38	2	1.69	4.71	0.0179	0.41
	f^2	51.81	1	51.81	144.64	<0.0001	6.03
	a_p^2	8.17	1	8.17	22.81	<0.0001	0.98
	$\in$	9.31	26	0.3582			1.12
	Total	832.15	38				100.00

Table 4
ANOVA results of surface roughness (R_a).

Response	Source	SS	DF	MS	F-value	p-value	PC
	V_c	0.7211	1	0.7211	45.81	<0.0001	14.57
	F	1.03	1	1.03	44.67	<0.0001	20.81
	a_p	0.3601	1	0.3601	64.02	<0.0001	7.27
	CA	2.22	2	1.11	22.31	<0.0001	44.85
	f^2	0.1018	1	0.1018	68.77	<0.0001	2.06
	$\in$	0.5165	32	0.0161	6.31	0.0173	10.44
	Total	4.95	38				100.00

For this study, $\gamma_k = 0.01, 0.03, 0.05, 0.07, 0.1, 0.2, 0.5, 1.0, 1.5$, and 2.0 were assumed. After imposing γ_k values, the changed weights of responses were recalculated for finding out the new sequence of ranking of alternatives.

3. Results and discussions

The objective of this study is to optimize the milling process by defining the relationship between input and response variables mathematically. Based on BBD design matrix, 39 experiment runs were carried out considering speed (V_c), feed rate (f), depth of cut (a_p), and cooling approach (CA) as input variables. The categorical variable cooling approach (CA) was symbolically presented for simplicity in computation where '1, 2, 3' were used for dry, HPC, and RHPC, respectively. Table 1 collects the results of multiple responses corresponding to experimental runs.

Mathematical models of F_c, SCE, and R_a were developed by using statistical software 'Design Expert' as presented in Eqns. 15–23. The selection of appropriate mathematical models is dependent on the value of determination of coefficient (R^2). Higher value of R^2 indicates the better predictability of any developed model [36]. The reported R^2 values of the quadratic models for F_c, SCE, and R_a were 0.98, 0.99, and 0.90. Additionally, the Predicted R^2 values of 0.96, 0.97, and 0.90 are consistent with the Adjusted R^2 values of 0.97, 0.98, and 0.90 for F_c, SCE, and R_a, respectively; the variation between this two is less than 0.2. The signal-to-noise ratio was measured by 'adequate precision' and this ratio greater than 4 is ideal, for F_c, SCE, and R_a which are 45.73, 47.89, and 25.09, respectively, suggest a sufficient signal, and the produced models can be utilized to navigate the design space. Another crucial factor, coefficient of variation, denoted by C_v represents the degree to which experimental results for any specified response are close to their mean [45]. C_v values of F_c, SCE, and R_a were 4.00%, 5.09%, and 10.02%, respectively. The lower value of C_v for F_c compared to other twos indicates that the variance with mean is the lowest.

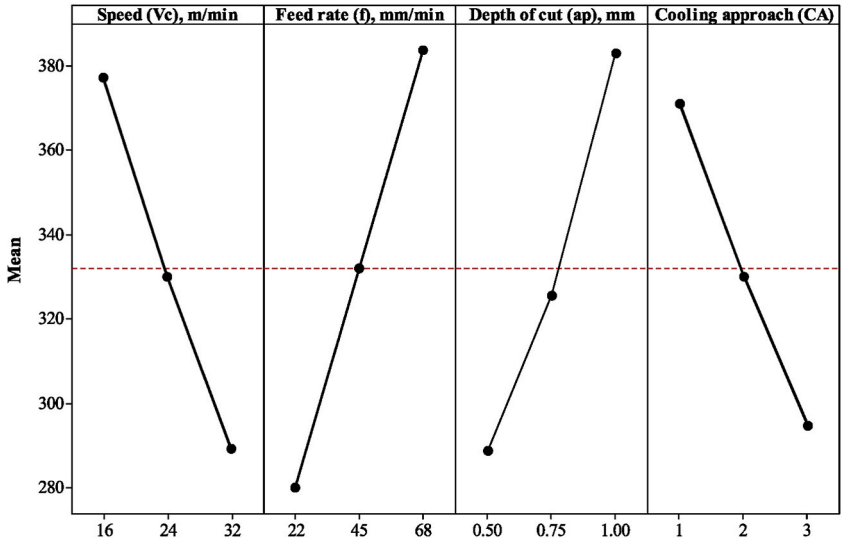

Fig. 4. Main effect plot for cutting force (F_c).

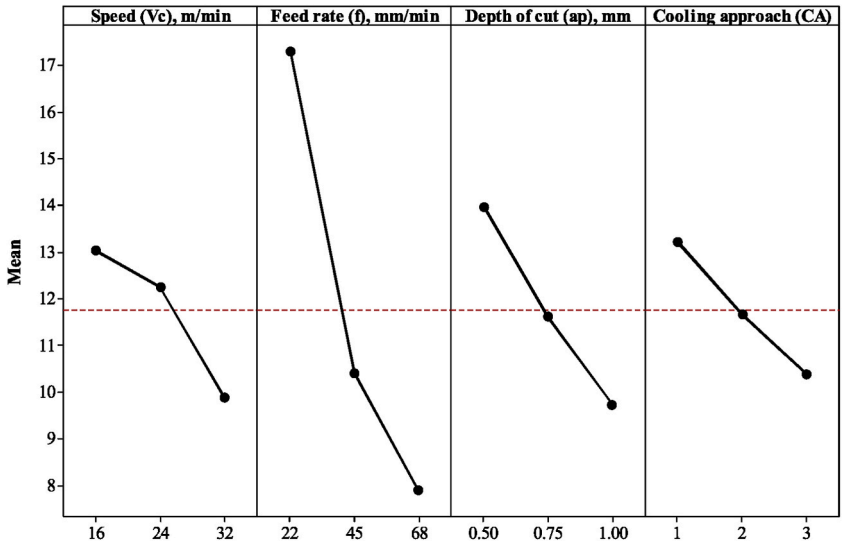

Fig. 5. Main effect plot for specific cutting energy (SCE).

$$F_c^1 = 173.96 - 2.84V_c + 4.66f + 172.2a_p - 3.54(V_c \times a_p) - 3.20(f \times a_p) + 163.73a_p^2; \quad (15)$$

$$F_c^2 = 133.04 - 2.84V_c + 4.66f + 172.2a_p - 3.54(V_c \times a_p) - 3.20(f \times a_p) + 163.73a_p^2; \quad (16)$$

$$F_c^3 = 97.8 - 2.84V_c + 4.66f + 172.2a_p - 3.54(V_c \times a_p) - 3.20(f \times a_p) + 163.73a_p^2; \quad (17)$$

$$SCE_c^1 = 57.87 - 0.43V_c - 0.78f - 33.73a_p + 0.005(V_c \times f) + 0.004f^2 + 15.8a_p^2; \quad (18)$$

$$SCE_c^2 = 53.7 - 0.43V_c - 0.78f - 33.73a_p + 0.005(V_c \times f) + 0.004f^2 + 15.8a_p^2; \quad (19)$$

$$SCE_c^3 = 49.9 - 0.43V_c - 0.78f - 33.73a_p + 0.005(V_c \times f) + 0.004f^2 + 15.8a_p^2; \quad (20)$$

$$R_a^1 = R_a = 1.67 - 0.022V_c - 0.009f - 0.49a_p + 0.0002f^2 + 1.22a_p^2; \quad (21)$$

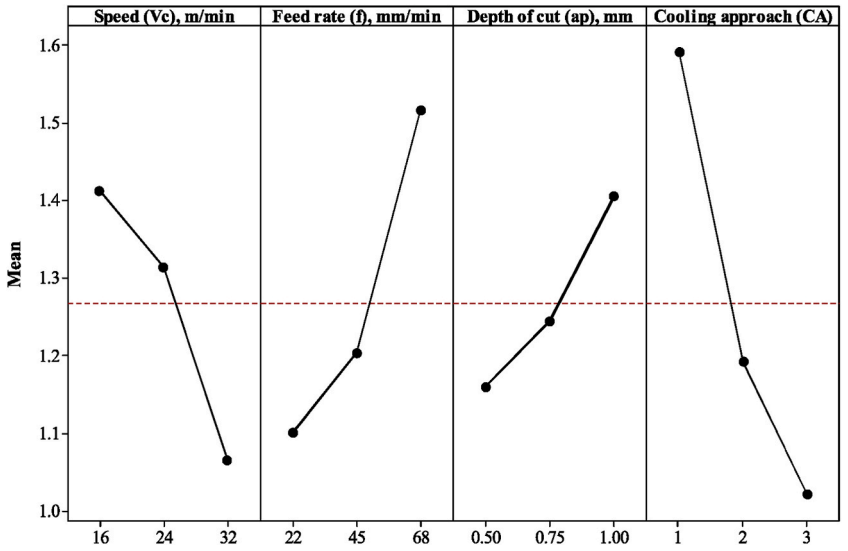

Fig. 6. Main effect plot for surface roughness (R_a).

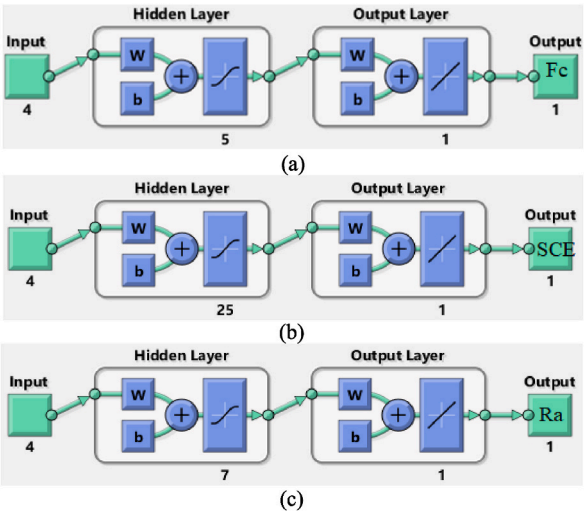

Fig. 7. ANN structure for (a) F_c, (b) SCE, and (c) R_a with selected hidden neurons.

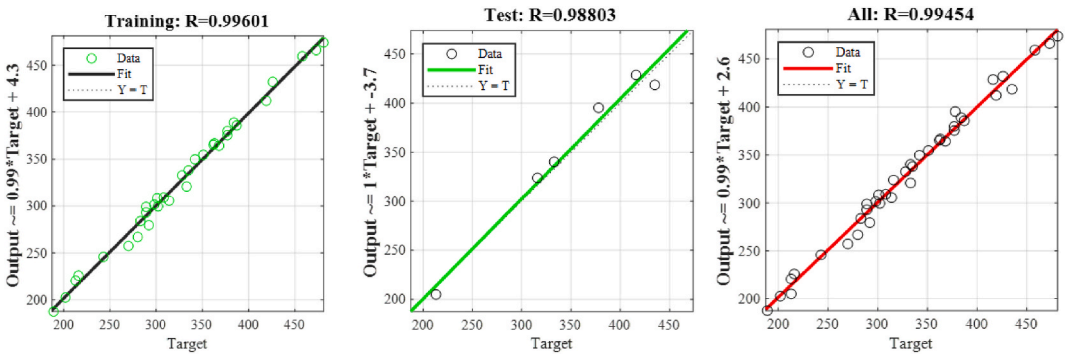

Fig. 8. Regression plots for F_c.

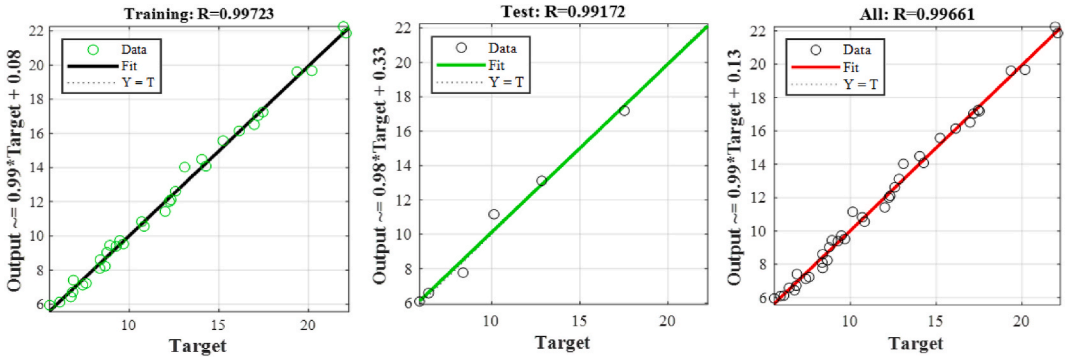

Fig. 9. Regression plots for SCE.

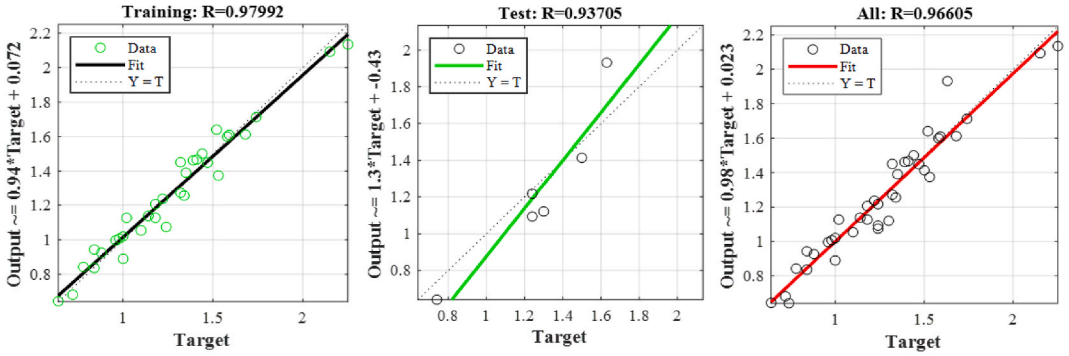

Fig. 10. Regression plots for R_a.

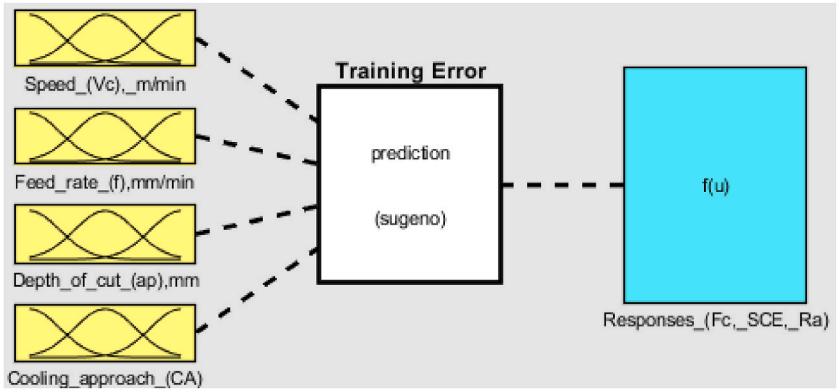

Fig. 11. Sugeno type ANFIS structure for modelling responses.

$$R_a^2 = 1.28 - 0.022V_c - 0.009f - 0.49a_p + 0.0002f^2 + 1.22a_p^2; \quad (22)$$

$$R_a^3 = 1.10 - 0.022V_c - 0.009f - 0.49a_p + 0.0002f^2 + 1.22a_p^2; \quad (23)$$

***Superscript 1, 2, 3 on the left side of the equations represents the cooling approach-dry, HPC and RHPC, respectively.

To predict the effect of process parameters on changing F_c, SCE, and R_a, ANOVA analysis of the developed models was carried out. Insignificant terms from the statistical analysis were subtracted by using the 'Backward elimination approach' to improve the model's accuracy within a 95% confidence level. Table 2 summarizes the ANOVA results for F_c with the percentage contribution of each input variable. In respect of F_c, linear terms, feed rate has the greatest effect (30.27%), followed by the depth of cut (25.06%), and cutting speed (20.88%). Cooling approach has the least effect (15.73%) on F_c comparative to others. Similarly, ANOVA analysis for SCE is collected in Table 3. Like F_c, for SCE, feed rate was noticed as the highest significant input variable with 63.3% contribution in

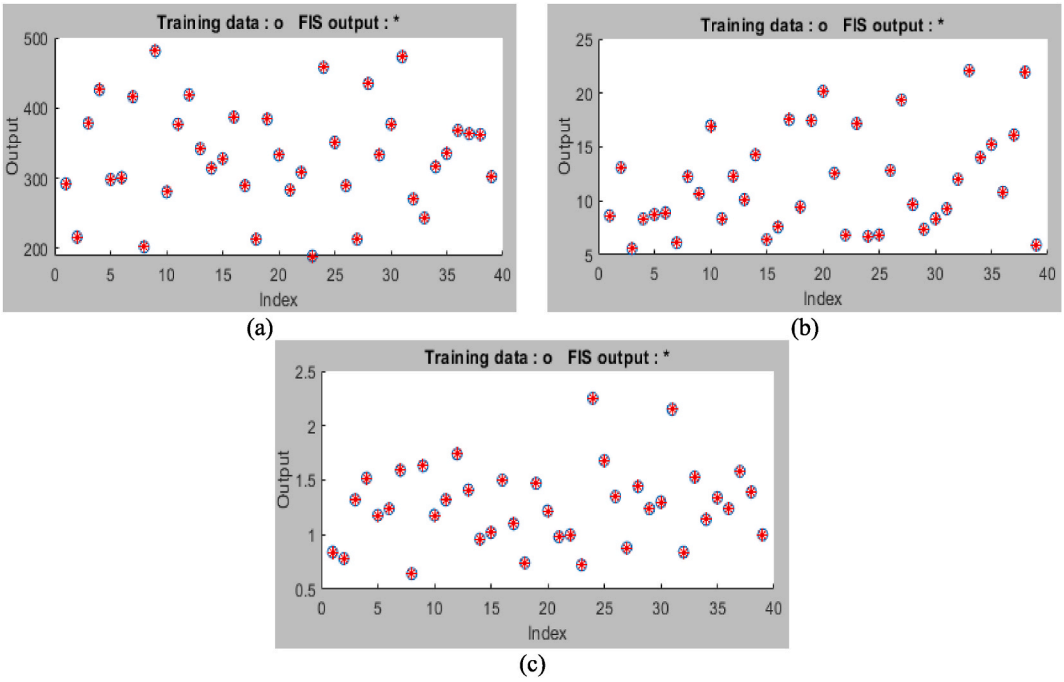

Fig. 12. Training datasets of (a) F_c, (b) SCE, and (c) R_a.

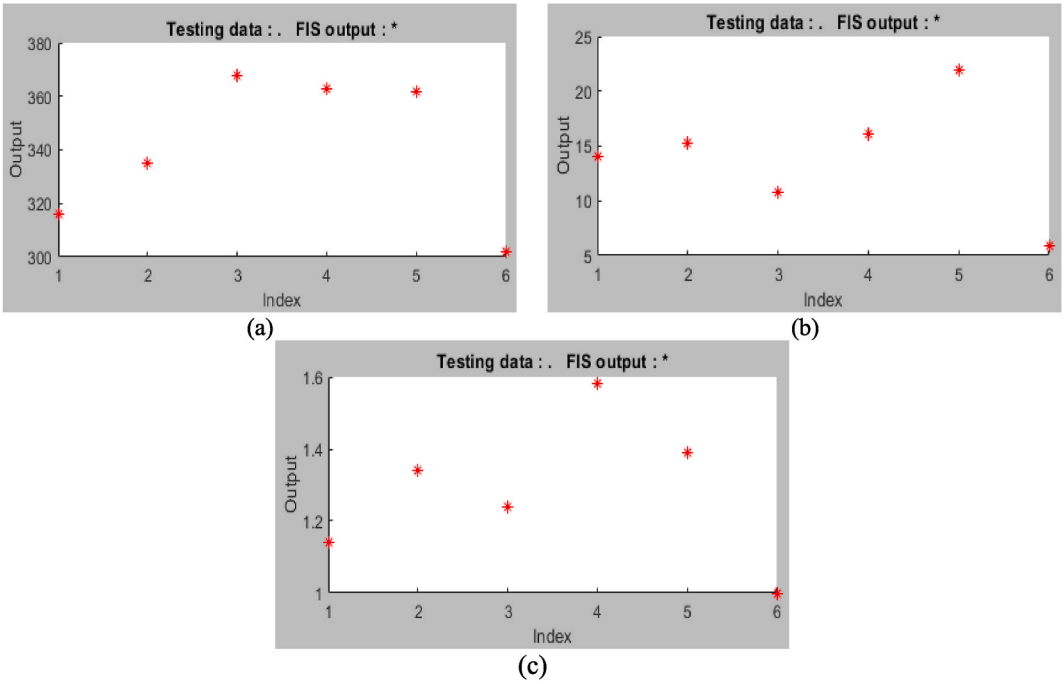

Fig. 13. Testing process results for (a) F_c, (b) SCE, and (c) R_a.

changing response followed by the depth of cut (12.64%), speed (7.12%), and lastly by the cooling approach (6.31%). Like F_c and SCE, all the linear input variables are significant in changing R_a. However, the insight of the percent contribution value reveals the cooling approach as the highest impactful element, among the studied factors. In terms of role (as presented in Table 4), next to cooling approach (44.85%), are the feed rate (20.81%), cutting speed (14.57%), and lastly, the depth of cut (7.27%). The application of RHPC in milling enhances the fluid penetration between tool-work interfaces that accredits to the reduction of rubbing action as well as the

Table 5
Statistical error analysis of RSM, ANN, and ANFIS.

Trial runs	APE values for RSM predicted results of-			APE values for ANN predicted results of-			APE values for ANFIS predicted results of-		
	F_c	SCE	R_a	F_c	SCE	R_a	F_c	SCE	R_a
1	1.21	4.68	13.92	4.28	4.83	12.32	0.0172	0.0214	0.1190
2	5.50	6.98	9.12	4.54	7.18	8.01	0.0092	0.0069	0.1282
3	0.34	6.62	5.45	4.58	7.02	3.60	0.0263	0.0212	0.1515
4	1.52	2.72	6.11	1.42	2.93	7.91	0.0048	0.0352	0.0658
5	7.98	4.53	2.81	1.18	3.07	4.45	0.0337	0.0537	0.0847
6	7.54	6.83	9.12	2.43	5.92	13.34	0.0101	0.0166	0.1613
7	0.36	2.21	1.77	3.02	0.06	1.28	0.0410	0.0384	0.0629
8	4.63	1.11	6.42	0.30	1.89	0.56	0.0348	0.0198	0.1563
9	1.64	4.14	11.78	1.47	1.35	18.49	0.0147	0.0104	0.0613
10	4.00	3.07	5.96	4.69	2.67	2.25	0.0035	0.0018	0.1695
11	1.61	4.80	11.77	0.38	7.29	9.93	0.0052	0.0265	0.0758
12	5.03	5.34	1.37	1.64	1.71	1.54	0.0240	0.0286	0.0575
13	6.62	9.38	8.24	2.30	10.15	4.05	0.0381	0.0329	0.7092
14	0.49	0.01	1.76	2.69	1.31	3.83	0.0126	0.0191	0.1042
15	1.08	6.70	24.13	1.43	2.46	10.52	0.0214	0.0213	0.9804
16	0.70	5.25	3.81	0.31	4.78	5.74	0.0130	0.0233	0.6667
17	2.89	0.51	6.56	3.44	1.89	4.15	0.0103	0.0277	0.9091
18	0.76	2.05	10.66	3.48	2.79	13.33	0.0470	0.0352	0.1351
19	1.20	0.08	5.18	1.28	1.11	1.43	0.0051	0.0260	0.0680
20	5.14	5.60	1.82	3.68	2.53	1.42	0.0361	0.0090	0.1639
21	1.93	1.19	2.84	0.33	0.32	2.83	0.0034	0.0177	0.1020
22	4.29	11.79	9.39	0.31	1.88	11.05	0.0064	0.0650	1.0000
23	4.08	1.89	1.65	0.79	0.79	5.39	0.0530	0.0106	0.2778
24	0.56	1.54	12.84	0.30	4.46	5.15	0.0198	0.0698	0.0889
25	6.11	9.42	0.88	1.04	7.71	4.03	0.0115	0.0342	0.0595
26	0.62	1.28	8.87	1.38	2.18	3.02	0.0036	0.0346	0.0741
27	1.65	1.96	2.49	3.80	1.27	5.17	0.0423	0.0188	0.1136
28	0.65	2.04	1.19	3.79	1.49	4.23	0.0231	0.0345	0.1389
29	0.89	9.34	13.22	2.19	3.69	11.83	0.0151	0.0000	0.0806
30	5.29	9.74	3.63	0.76	2.66	13.82	0.0240	0.0265	2.3077
31	2.65	5.18	6.42	1.47	1.38	2.65	0.0212	0.0486	0.0465
32	7.46	6.97	1.06	4.69	4.80	0.43	0.0371	0.0000	0.3571
33	5.94	1.74	14.95	1.15	1.06	10.17	0.1400	0.0041	0.0654
34	2.43	1.96	3.32	2.48	3.19	0.15	0.0126	0.0317	0.1754
35	3.79	0.39	14.41	0.92	2.27	6.28	0.0029	0.0179	0.1493
36	2.98	1.07	6.20	1.02	2.37	1.81	0.2447	0.0326	0.0806
37	0.44	0.20	0.19	1.02	0.09	1.24	0.2480	0.0207	0.0633
38	1.44	2.02	14.89	0.92	1.38	5.17	0.0277	0.0028	0.1439
39	1.88	0.08	9.61	0.84	3.02	2.03	0.0034	0.0265	1.0000
MAPE	**2.957**	**3.908**	**7.072**	**1.993**	**3.050**	**5.759**	**0.035**	**0.024**	**0.025**

reduction of tool wear through the proper controlling of temperature rise and therefore, is possible to reduce roughness significantly.

Fig. 4 shows the main effect plot for F_c regarding the variation of input variables at different levels. From the main effect plot it is visible that, the minimum cutting force was achieved at 32 m/min speed, 22 mm/min feed rate, and 0.50 mm depth of cut with RHPC. The explanation can be given by mentioning Johnson-Cook's flow stress model [46]. This material model states that the strain rate, strain hardening, and thermal softening effect significantly affects the flow stress behaviour of material. In case of machining Ti–6Al–4V alloy, thermal softening occurs at higher speed because of enhanced heat generation that positively affects in reducing cutting force. On the other hand, at higher feed rate and depth of cut, the chip load increases at each tool tip of the cutter that raises up the cutting force. Beside those parameters, proper cooling and lubrication effect of RHPC reduces cutting force significantly.

From Fig. 5, minimum specific cutting energy (SCE) was noticed at 32 m/min speed, 68 mm/min feed rate, and 1.00 mm depth of cut with RHPC. At higher cutting speed, lower SCE was accredited by the reduced cutting force with thermal softening and less built-up edge formation. The inverse relationship between specific cutting energy and feed rate as well as depth of cut can be justified by the mathematical relation expressed in Eqn. (1). The higher reduction rate of SCE in RHPC reduced compared to HPC reveals the better cooling and lubrication behaviour of RHPC.

Like cutting force, lower surface roughness was achieved for milling under RHPC at 32 m/min speed, 22 mm/min feed rate and 0.50 mm depth of cut, as shown in Fig. 6. With increased speed, the less formation of BUE ultimately minimizes surface roughness. Moreover, at higher speed, the coefficient of friction is reduced that is also reported by another research study [47]. But, at higher feed rate and depth of cut, the increased cutting pressure reduced the surface quality of the finished product.

The feed forward back propagation type ANN network for each response was trained with Bayesian regularization (TrainBr) algorithm considering 33 alternatives for 1000 epochs and tested for 6 alternatives. After trial and error, 5, 25, and 7 neurons in the hidden layer was set for constructing the optimized ANN models of F_c, SCE, and R_a, respectively, as shown in Fig. 7. Figs. 8, 9 and 10show the regression plots for F_c, SCE, and R_a that also reveals the higher accuracy of the selected models because most of the points

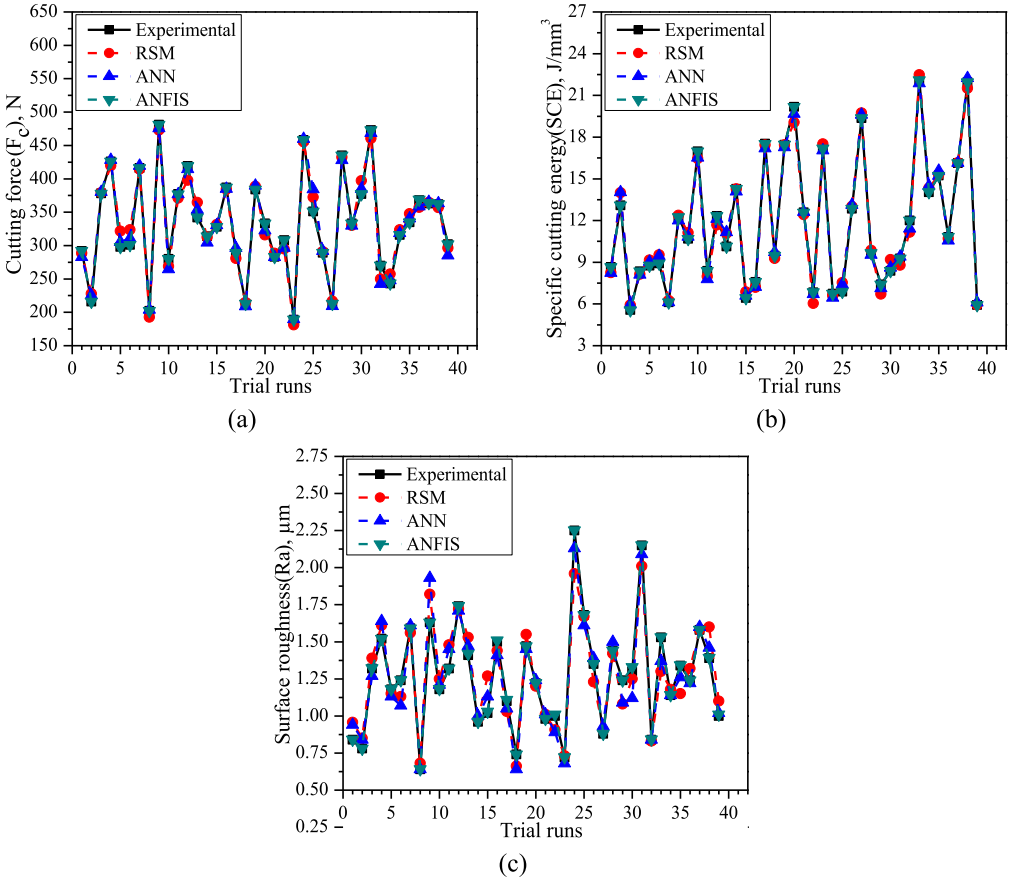

Fig. 14. Comparative study of RSM, ANN, and ANFIS models in predicting (a) F_c, (b) SCE, and (c)R_a.

Table 6
PCA derived relative weights of selected criteria for the current study.

Criteria	Cutting force	Specific cutting energy	Surface roughness
Weights	0.46	0.13	0.41

fit very well with the line except a few points. The calculated values of coefficient of determination (R^2) for the trained ANN models of F_c, SCE, and R_a were 0.99601, 0.99723, and 0.97992, respectively. All the measured values of R^2 are higher than 0.90 that also depicts the model accuracy. Furthermore, for training and test data sets, the predicted results fit very well with the 45-degree line especially that also manifests that the selected specific ANN output network was adequate in describing the selected responses F_c, SCE, and R_a (see).

Like RSM and ANN, the ANFIS structure was used to predict responses of the given dataset in Table 1. The initiation of ANFIS analysis was carried out by the formation of 39 × 5 matrix that actually signifies the presence of four inputs with a single output for 39 trial runs as shown in Fig. 11. Sugeno type FIS structure was chosen because of its better processing time with the weighted average defuzzification.

For analysis, Grid partition technique was adopted to generate the optimized rules considering triangular membership functions (trimf). Hybrid optimization method with 0 error tolerances was carried out for 100 epochs after loading training and test datasets that comprises of the least square method and the gradient descent method. Fig. 12 shows the model outcomes of F_c, SCE, and R_a with their experimental results under the same processing conditions for showing the discrepancies between those actual and predicted datasets in the training process. For training datasets of F_c, SCE, and R_a by using ANFIS model, the minimum RMSE values were achieved as 0.00339, 0.000013, and 0.000001 that manifests the higher prediction accuracy of the used model. Finally, the validation was checked out by the testing process and the testing results are shown in Fig. 13. The estimated coefficients of determination (R^2) for F_c, SCE, and R_a were 0.9999, 0.9998 and 0.9768, respectively reveal the model's higher prediction accuracy.

Different degrees of prediction accuracy were noticed for each prediction model (RSM, ANN, ANFIS) and hence, to declare the best prediction model in this specific case, the statistical error analysis was carried out following APE and MAPE. Table 5 summarizes the

Table 7
Selection of the best alternative based on PCA-MOORA method.

Alternatives	Normalized values of-			Weighted normalized values of-			Performance score	Rank
	F_c	SCE	R_a	F_c	SCE	R_a		
A1	0.1375	0.1097	0.1021	0.0636	0.0142	0.0416	−0.1194	5
A2	0.1017	0.1660	0.0948	0.0470	0.0215	0.0386	−0.1071	4
A3	0.1780	0.0705	0.1605	0.0823	0.0091	0.0653	−0.1568	20
A4	0.2006	0.1059	0.1848	0.0928	0.0137	0.0752	−0.1817	31
A5	0.1403	0.1111	0.1435	0.0649	0.0144	0.0584	−0.1377	12
A6	0.1417	0.1131	0.1508	0.0655	0.0147	0.0614	−0.1416	14
A7	0.1959	0.0776	0.1933	0.0906	0.0101	0.0787	−0.1793	30
A8	0.0951	0.1552	0.0778	0.0440	0.0201	0.0317	−0.0958	1*
A9	0.2265	0.1355	0.1982	0.1047	0.0176	0.0807	−0.2030	37
A10	0.1319	0.2152	0.1435	0.0610	0.0279	0.0584	−0.1473	17
A11	0.1775	0.1062	0.1605	0.0821	0.0138	0.0653	−0.1612	24
A12	0.1973	0.1562	0.2115	0.0912	0.0202	0.0861	−0.1976	36
A13	0.1611	0.1285	0.1714	0.0745	0.0167	0.0698	−0.1609	23
A14	0.1479	0.1810	0.1167	0.0684	0.0235	0.0475	−0.1393	13
A15	0.1545	0.0815	0.1240	0.0714	0.0106	0.0505	−0.1325	11
A16	0.1822	0.0962	0.1824	0.0843	0.0125	0.0742	−0.1710	29
A17	0.1361	0.2221	0.1337	0.0629	0.0288	0.0544	−0.1461	16
A18	0.1003	0.1200	0.0900	0.0464	0.0156	0.0366	−0.0986	2
A19	0.1808	0.2213	0.1787	0.0836	0.0287	0.0727	−0.1850	35
A20	0.1568	0.2559	0.1483	0.0725	0.0332	0.0604	−0.1661	27
A21	0.1333	0.1595	0.1191	0.0616	0.0207	0.0485	−0.1308	10
A22	0.1450	0.0868	0.1216	0.0671	0.0112	0.0495	−0.1278	9
A23	0.0890	0.2178	0.0875	0.0412	0.0282	0.0356	−0.1050	3
A24	0.2157	0.0854	0.2736	0.0997	0.0111	0.1113	−0.2221	38
A25	0.1653	0.0873	0.2043	0.0764	0.0113	0.0831	−0.1709	28
A26	0.1361	0.1629	0.1641	0.0629	0.0211	0.0668	−0.1508	19
A27	0.1003	0.2455	0.1070	0.0464	0.0318	0.0435	−0.1217	7
A28	0.2049	0.1226	0.1751	0.0947	0.0159	0.0713	−0.1819	32
A29	0.1568	0.0938	0.1508	0.0725	0.0122	0.0614	−0.1460	15
A30	0.1775	0.1062	0.1581	0.0821	0.0138	0.0643	−0.1602	22
A31	0.2227	0.1176	0.2614	0.1030	0.0152	0.1064	−0.2246	39
A32	0.1272	0.1521	0.1021	0.0588	0.0197	0.0416	−0.1201	6
A33	0.1144	0.2801	0.1860	0.0529	0.0363	0.0757	−0.1649	26
A34	0.1488	0.1781	0.1386	0.0688	0.0231	0.0564	−0.1483	18
A35	0.1578	0.1931	0.1629	0.0729	0.0250	0.0663	−0.1643	25
A36	0.1733	0.1372	0.1508	0.0801	0.0178	0.0614	−0.1593	21
A37	0.1709	0.2046	0.1921	0.0790	0.0265	0.0782	−0.1837	34
A38	0.1705	0.2782	0.1690	0.0788	0.0360	0.0688	−0.1837	33
A39	0.1422	0.0751	0.1216	0.0658	0.0097	0.0495	−0.1250	8

* Represents the optimal solution

Table 8
Changed criteria weights with the imposed disturbances.

Unitary ratio (γ_k, k = F_c, SCE, R_a)	Weights of criteria due to disturbance induced on cutting force (F_c)			Weights of criteria due to disturbance induced on specific cutting energy (SCE)			Weights of criteria due to disturbance induced on surface roughness (R_a)		
	F_c	SCE	R_a	SCE	F_c	R_a	R_a	F_c	SCE
0.01	0.005	0.240	0.756	0.001	0.528	0.471	0.004	0.776	0.219
0.03	0.014	0.237	0.749	0.004	0.527	0.469	0.0123	0.770	0.218
0.05	0.023	0.235	0.742	0.007	0.525	0.468	0.0205	0.764	0.216
0.07	0.032	0.233	0.735	0.009	0.524	0.467	0.0287	0.757	0.214
0.1	0.046	0.230	0.724	0.013	0.522	0.465	0.041	0.748	0.211
0.2	0.092	0.219	0.689	0.026	0.515	0.459	0.082	0.716	0.202
0.5	0.230	0.185	0.585	0.065	0.494	0.441	0.205	0.620	0.175
1.0	0.460	0.130	0.410	0.130	0.460	0.410	0.41	0.460	0.130
1.5	0.690	0.075	0.235	0.195	0.426	0.379	0.615	0.300	0.085
2.0	0.920	0.019	0.061	0.260	0.391	0.349	0.82	0.140	0.040

suggested models' predictability for 39 experimental trials. The statistical analysis reveals no significant discrepancies between used models in predicting the machinability characteristics. However, from the tabulated results, the ANN and ANFIS models seem to be more appropriate compared to RSM models. Such results also agreed with the prior study results [48]. As the error results are within 10%, it can be claimed that the selected models are capable to accurately predict the results. The comparative analysis is also

Table 9
Ranking of alternatives with the imposed disturbances on cutting force (F_c).

	Ranking due to the change of unitary ratios (γ_{Fc})									
Alternatives	**0.01**	**0.03**	**0.05**	**0.07**	**0.1**	**0.2**	**0.5**	**1.0**	**1.5**	**2.0**
A1	3	3	3	3	3	3	4	5	7	10
A2	5	5	5	5	4	4	3	4	4	4
A3	14	14	15	15	15	16	16	20	25	28
A4	28	28	28	28	28	28	31	31	34	35
A5	12	12	12	12	12	12	13	12	11	14
A6	16	16	16	16	16	15	15	14	13	15
A7	27	27	27	27	27	27	29	30	33	33
A8	1	1	1	1	1	1	1	1	1	2
A9	32	32	32	32	32	32	36	37	37	38
A10	22	22	22	22	22	22	21	17	12	9
A11	18	18	19	20	20	20	22	24	27	30
A12	36	36	36	36	36	36	37	36	36	34
A13	23	23	23	23	23	23	24	23	21	23
A14	11	11	11	11	11	11	12	13	16	17
A15	7	8	8	8	8	9	9	11	14	19
A16	24	24	24	24	25	25	25	28	29	31
A17	21	21	21	21	21	21	18	16	15	11
A18	2	2	2	2	2	2	2	2	3	3
A19	33	33	33	33	33	33	33	35	32	32
A20	30	30	30	30	30	30	27	27	23	21
A21	10	10	10	10	10	10	10	10	8	8
A22	6	6	6	6	6	7	8	9	10	16
A23	9	9	9	9	9	8	5	3	2	1
A24	39	39	39	39	39	39	38	38	38	37
A25	31	31	31	31	31	31	30	29	28	24
A26	26	26	25	25	24	24	23	19	18	12
A27	15	15	14	14	14	13	11	7	5	5
A28	25	25	26	26	26	26	28	32	35	36
A29	13	13	13	13	13	14	14	15	20	20
A30	17	17	17	17	17	18	19	22	26	29
A31	38	38	38	38	38	38	39	39	39	39
A32	8	7	7	7	7	6	6	6	6	7
A33	37	37	37	37	37	37	32	26	17	6
A34	20	20	20	18	18	17	17	18	19	18
A35	29	29	29	29	29	29	26	25	22	22
A36	19	19	18	19	19	19	20	21	24	25
A37	34	34	34	34	34	34	34	34	31	27
A38	35	35	35	35	35	35	35	33	30	26
A39	4	4	4	4	5	5	7	8	9	13

graphically shown in Fig. 14.

With the criteria weights derived by PCA as presented in Table 6, the MOORA method was applied to optimize the selected responses. Table 7 represents the optimization results with the indication of best alternatives. It can be observed that alternative A8 at 32 m/min speed, 22 mm/min feed rate, and 0.75 mm depth of cut under RHPC was selected as the best alternative with the highest weighted assessment value.

After selecting the best alternatives, the next step was to conduct the sensitivity analysis with the variation of unitary ratio of the criteria weights. Table 8 shows the changed criteria weights $w_k^{'}$ with the variation of unitary ratios γ_k. The sensitivity of each alternative's ranking with the imposed disturbances on the PCA derived weightages of cutting force, specific cutting energy, and surface roughness, respectively are summarized in Tables 9–11. As can be seen in Table 9, the variation of the ranking alternatives was consistent for the lower range of unitary ratio (γ_{Fc}) at 0.01–0.07. After, $\gamma_{Fc} = 0.2$ the change of ranking sequence became more unpredictable. The optimal alternative was noticed insensitive for γ_{Fc} up to 1.5. Table 10 shows the variation of weightages for specific cutting energy. Severe inconsistency of ranking sequence was not noticed for the unitary ratio γ_{SCE} reaching up to 0.2. Above this value of unitary ratio, the alteration of ranking sequence was found to be more irregular. The selection of optimal alternative was changed when γ_{SCE} reached above 1.5. Lastly, Table 11 lists the sequence of ranking alternatives for changing weightages of surface roughness. No sharp deviations of ranking sequence were observed. But, alternative A8 was selected as the best optimal alternative like PCA-MOORA after considering the imposed unitary ratio γ_{Ra} within 0.5–2.0 that indicates the higher sensitivity of surface roughness with the lower value of $\gamma_{Ra.}$ For clear understanding concerning this, a graphical analysis was carried out, as shown in Fig. 15. From the graphical plot, it has been observed that for cutting force, the sensitivity of ranking derived from PCA-MOORA was higher compared to specific cutting energy, and surface roughness. Actually, imposed disturbances affected it more because the weightage of cutting force derived by PCA was higher than the other twos.

Table 10
Ranking of alternatives with the imposed disturbances on specific cutting energy (SCE).

Alternatives	Ranking due to the change of unitary ratios (γ_{SCE})									
	0.01	0.03	0.05	0.07	0.1	0.2	0.5	1.0	1.5	2.0
A1	7	7	7	7	7	7	7	5	5	5
A2	4	4	4	4	4	4	4	4	3	3
A3	27	27	27	26	26	26	24	20	16	15
A4	34	34	34	34	34	34	35	31	31	29
A5	15	15	15	15	15	15	13	12	12	10
A6	17	17	17	17	17	17	16	14	13	12
A7	35	35	35	35	35	35	34	30	28	27
A8	1	1	1	1	1	1	1	1	2	2
A9	37	37	37	37	37	37	37	37	37	36
A10	13	13	13	13	13	14	15	17	20	23
A11	26	26	26	27	27	27	27	24	22	20
A12	36	36	36	36	36	36	36	36	36	35
A13	24	24	24	24	24	24	25	23	24	22
A14	10	10	10	11	11	11	11	13	15	16
A15	14	14	14	14	14	13	12	11	9	8
A16	31	31	31	31	30	29	28	28	26	26
A17	12	12	12	12	12	12	14	16	19	24
A18	3	3	3	3	3	3	3	2	1	1
A19	29	29	29	29	29	30	32	35	34	34
A20	20	20	20	21	21	21	21	27	29	31
A21	8	8	8	8	8	8	8	10	11	11
A22	11	11	11	10	10	10	10	9	8	6
A23	2	2	2	2	2	2	2	3	4	7
A24	39	39	39	39	39	39	38	38	38	38
A25	32	32	32	32	32	31	30	29	25	25
A26	19	19	19	19	18	18	19	19	18	18
A27	5	5	5	5	5	5	5	7	10	14
A28	33	33	33	33	33	33	33	32	32	30
A29	21	21	21	20	20	20	18	15	14	13
A30	25	25	25	25	25	25	26	22	21	17
A31	38	38	38	38	38	38	39	39	39	39
A32	6	6	6	6	6	6	6	6	7	9
A33	18	18	18	18	19	19	20	26	30	32
A34	16	16	16	16	16	16	17	18	17	19
A35	22	22	22	22	22	22	23	25	27	28
A36	23	23	23	23	23	23	22	21	23	21
A37	30	30	30	30	31	32	31	34	33	33
A38	28	28	28	28	28	28	29	33	35	37
A39	9	9	9	9	9	9	9	8	6	4

4. Conclusions and limitations of the study

From the mathematical model development, comparison, optimization, and sensitivity analysis, the following conclusions can be drawn.

- The present study explores the novel use of rotary applicator for spraying high-pressure coolant jets targeting the tool tip of complex helix shaped end mill cutter. Forced convective heat transfer mechanism of this modified design enhanced the cooling rate that results comparatively better machinability than conventional HPC. RHPC reduced cutting force, specific energy consumption, and surface roughness by 10.60%, 10.61%, and 14.36% respectively compared to HPC.
- Based on the determination of coefficients (R^2, adjusted R^2, predicted R^2), the developed RSM models for predicting responses such as cutting force, specific cutting energy, and surface roughness were found to be satisfactory. All of the coefficients were greater than 90%, indicating that the derived models described more than 90% of the variability in the response data. As a whole, these models are highly favorable.
- ANOVA results divulged that the feed rate has the greatest effect on modifying the value of cutting force and specific cutting energy, whereas the cooling strategy has the most dominant effect on surface roughness variation.
- Main effects plots revealed that the minimum cutting force and surface roughness were found to be prompted by the high-pressure coolant condition, cutting speed of 32 m/min, feed rate of 22, and depth of cut of 0.50 mm; the minimum specific cutting energy required the highest feed rate (68 mm/min) and depth of cut (1.0 mm), not the lowest feed rate and depth of cut along with similar speed and cooling approach.
- For predicting responses such as cutting force, specific cutting energy, and surface roughness, feed forward back propagation type ANN networks with 4-5-1, 4-25-1, and 4-7-1 structures trained by Bayesian regularization were selected. The recommended ANN

Table 11
Ranking of alternatives with the imposed disturbances on roughness (R_a).

Alternatives	Ranking due to the change of unitary ratios (γ_{Ra})									
	0.01	0.03	0.05	0.07	0.1	0.2	0.5	1.0	1.5	2.0
A1	6	6	6	6	6	6	5	5	5	5
A2	3	3	3	3	3	3	4	4	4	4
A3	20	20	21	22	21	22	20	20	21	22
A4	32	32	32	32	32	32	31	31	32	32
A5	10	10	10	10	10	10	12	12	13	15
A6	11	11	11	11	11	11	13	14	15	17
A7	29	29	29	29	29	29	30	30	34	33
A8	2	2	2	2	2	2	2	1	1	1
A9	39	39	39	39	39	39	38	37	36	36
A10	17	17	17	17	16	16	17	17	17	16
A11	25	25	25	25	25	25	25	24	24	24
A12	35	35	34	34	34	35	36	36	37	37
A13	19	19	19	20	23	23	21	23	26	26
A14	22	21	20	19	19	17	16	13	12	11
A15	12	12	12	12	12	12	11	11	11	12
A16	26	26	26	26	26	27	28	28	28	29
A17	21	22	22	21	20	19	18	16	14	13
A18	1	1	1	1	1	1	1	2	2	2
A19	36	36	36	35	35	34	34	35	33	31
A20	31	30	30	30	30	30	29	27	23	20
A21	13	13	13	13	13	13	10	10	10	9
A22	7	8	8	9	9	9	9	9	9	10
A23	4	4	4	4	4	4	3	3	3	3
A24	34	34	35	36	36	37	37	38	39	39
A25	16	16	16	16	17	18	23	29	31	35
A26	14	14	14	14	14	15	15	19	19	23
A27	8	7	7	7	7	8	8	7	7	7
A28	33	33	33	33	33	33	33	32	30	28
A29	15	15	15	15	15	14	14	15	18	18
A30	24	24	24	24	24	24	24	22	22	21
A31	38	38	38	38	38	38	39	39	38	38
A32	9	9	9	8	8	7	7	6	6	6
A33	18	18	18	18	18	20	22	26	27	30
A34	23	23	23	23	22	21	19	18	16	14
A35	28	28	28	28	28	28	27	25	25	25
A36	27	27	27	27	27	26	26	21	20	19
A37	30	31	31	31	31	31	32	34	35	34
A38	37	37	37	37	37	36	35	33	29	27
A39	5	5	5	5	5	5	6	8	8	8

models of the specified responses have higher coefficients of determination (R^2) of 0.99601, 0.99723, and 0.97992, indicating its better predictability.

- Like RSM and ANN, ANFIS model was employed to predict responses and the calculated coefficients of determination (R^2) for cutting force, specific cutting energy, and surface roughness were 0.9999, 0.9998, and 0.9768, indicating the model's superior prediction accuracy.
- Comparative assessment of the used predictive models recommended ANFIS as the most accurate and precise way to anticipate responses with the lowest MAPE value.
- The PCA-MOORA optimization approach revealed that milling of Ti–6Al–4V alloy at a cutting speed of 32 m/min, feed rate of 22 mm/min, and 0.75 mm depth of cut under the application of high-pressure coolant jets by rotary applicator simultaneously optimize all the responses.
- Sensitivity analysis revealed that the deviation of the order of preference sequences is more irregular with the higher value of unitary ratio.

This study provides a substantial platform for sensitivity analysis of the PCA-MOORA approach in milling, and its use in the field of other machining processes can be significantly expanded. Furthermore, sensitivity analyses for additional multi-criteria decision models can be undertaken to determine the best decision model for a specific scenario.

Author contribution statement

MST.NAZMA SULTANA: Conceived and designed the experiments; Performed the experiments; Analyzed and interpreted the data; Wrote the paper.

Nikhil Ranjan Dhar: Contributed reagents, materials, analysis tools or data.

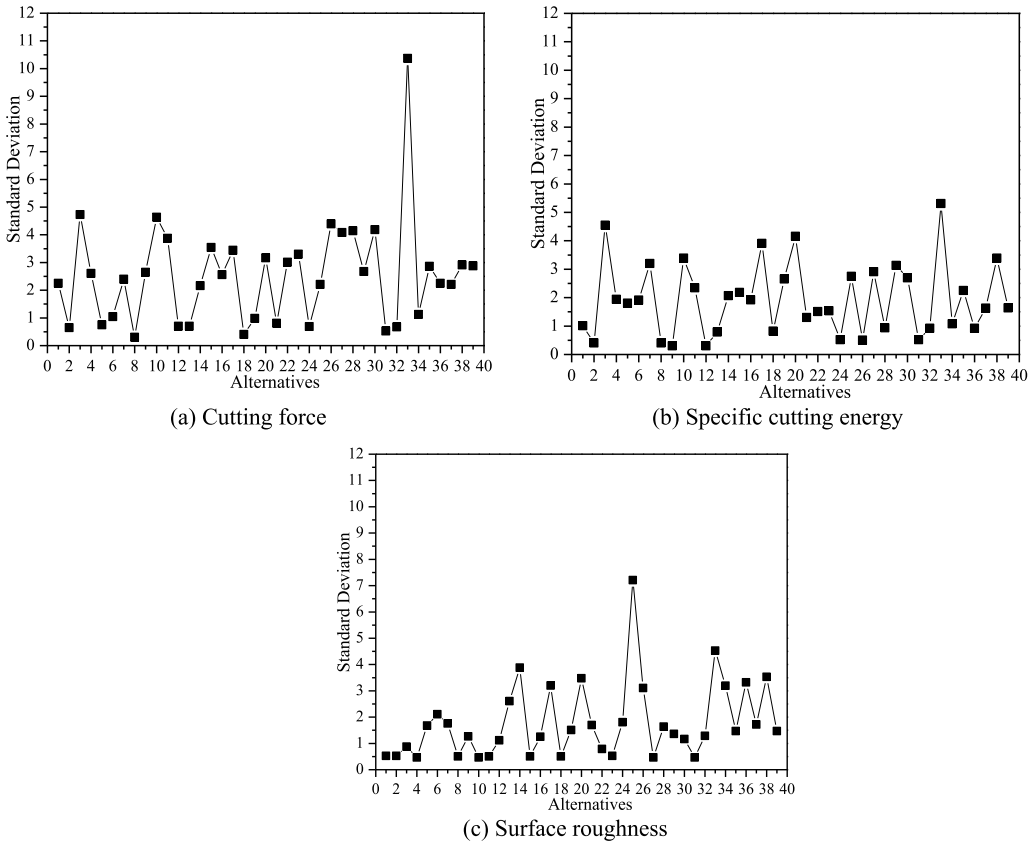

Fig. 15. Graphical plots for standard deviations of ranking alternatives due to variation of unitary ratios of (a) cutting force, (b) specific cutting energy, and (c) surface roughness.

Data availability statement

Data included in article/supplementary material/referenced in article.

Declaration of competing interest

The authors declare that they have no known competing financial interests or personal relationships that could have appeared to influence the work reported in this paper.

Acknowledgements

The authors would like to express their appreciation to the Ministry of National Science and Technology (NST), Dhaka, Bangladesh, Code No. 120005100–382117, GO No. 39.00.0000.012.002.05.20–04, Dated: January 10, 2021, for financially supporting this research. The authors would also like to acknowledge the Directorate of Advisory Extension and Research Services (DAERS) at BUET and the Department of Industrial and Production Engineering at BUET in Dhaka, Bangladesh for allowing us to conduct the research using their laboratory facilities.

References

[1] G.M. Pittalà, M. Monno, A new approach to the prediction of temperature of the workpiece of face milling operations of Ti-6Al-4V, Appl. Therm. Eng. 31 (2–3) (2011) 173–180, https://doi.org/10.1016/j.applthermaleng.2010.08.027.

[2] O.O. Daramola, I. Tlhabadira, J.L. Olajide, I.A. Daniyan, E.R. Sadiku, L. Masu, L.R. VanStaden, Process design for optimal minimization of resultant cutting force during the machining of Ti-6Al-4V: response surface method and desirability function analysis, Procedia CIRP 84 (2019) 854–860, https://doi.org/10.1016/j.procir.2019.04.185.

[3] S. Pervaiz, I. Deiab, B. Darras, Power consumption and tool wear assessment when machining titanium alloys, Int J Precis Eng 14 (6) (2013) 925–936, https://doi.org/10.1007/s12541-013-0122-y.

[4] N.E. Karkalos, N.I. Galanis, A.P. Markopoulos, Surface roughness prediction for the milling of Ti–6Al–4V ELI alloy with the use of statistical and soft computing techniques, Measurement 90 (2016) 25–35, https://doi.org/10.1016/j.measurement.2016.04.039.

[5] E.O. Ezugwu, Key improvements in the machining of difficult-to-cut aerospace superalloys, Int. J. Mach. Tool Manufact. 45 (12–13) (2005) 1353–1367, https://doi.org/10.1016/j.ijmachtools.2005.02.003.

[6] R. Peng, J. Liu, M. Chen, J. Tong, L. Zhao, Development of a pressurized internal cooling milling cutter and its machining performance assessment, Precis. Eng. 72 (2021) 315–329, https://doi.org/10.1016/j.precisioneng.2021.05.010.

[7] S. Shu, Y. Zhang, Y. He, H. Zhang, Design of a novel turning tool cooled by combining circulating internal cooling with spray cooling for green cutting, J Adv Mech Des Sys Manuf 15 (1) (2021) 1–11, https://doi.org/10.1299/jamdsm.2021jamdsm0003.

[8] S. Zhang, J.F. Li, J. Sun, F. Jiang, Tool wear and cutting forces variation in high-speed end-milling Ti-6Al-4V alloy, Int. J. Adv. Manuf. Technol. 46 (1) (2010) 69–78, https://doi.org/10.1007/s00170-009-2077-9.

[9] M. Mia, N.R. Dhar, Modelling of surface roughness using RSM, FL and SA in dry hard turning, Arabian J. Sci. Eng. 43 (3) (2018) 1125–1136, https://doi.org/10.1007/s13369-017-2754-1.

[10] M.A. Sulaiman, C.C. Haron, J.A. Ghani, M.S. Kasim, Effect of high-speed parameters on uncoated carbide tool in finish turning Titanium Ti-6Al-4V ELI, Sains Malays. 43 (1) (2014) 111–116.

[11] R. Shetty, C.R. Kumar, M.R. Ravindra, RSM based expert system development for cutting force prediction during machining of Ti–6Al–4V under minimum quantity lubrication, Int J Syst Assur Eng Manag 1–8 (2021), https://doi.org/10.1007/s13198-021-01495-z.

[12] K.H. Hashmi, G. Zakria, M.B. Raza, S. Khalil, Optimization of process parameters for high-speed machining of Ti-6Al-4V using response surface methodology, Int. J. Adv. Manuf. Technol. 85 (5) (2016) 1847–1856, https://doi.org/10.1007/s00170-015-8057-3.

[13] A.M. Zain, H. Haron, S. Sharif, Prediction of surface roughness in the end milling machining using Artificial Neural Network, Expert Syst. Appl. 37 (2) (2010) 1755–1768, https://doi.org/10.1016/j.eswa.2009.07.033.4.

[14] R.H. Namlu, C. Turhan, B.L. Sadigh, S.E. Kilic, Cutting force prediction in ultrasonic-assisted milling of Ti–6Al–4V with different machining conditions using artificial neural network, Artif Intell Eng Des Anal Man 35 (1) (2021) 37–48, https://doi.org/10.1017/S0890060420000360.

[15] S. Al-Zubaidi, J.A. Ghani, C.H. Che Haron, Prediction of surface roughness when end milling Ti6Al4V alloy using adaptive neuro-fuzzy inference system, Model. Simulat. Eng. 2013 (2013) 1–12, https://doi.org/10.1155/2013/932094.

[16] C. Bandapalli, B.M. Sutaria, D.V. Bhatt, Estimation of surface roughness on Ti-6Al-4V in high-speed micro end milling by ANFIS model, Indian J. Eng. Mater. Sci. 26 (2019) 379–389.

[17] E. Kilickap, A. Yardimeden, Y.H. Çelik, Mathematical modelling and optimization of cutting force, tool wear and surface roughness by using artificial neural network and response surface methodology in milling of Ti-6242S, Appl. Sci. 7 (10) (2017) 1064, https://doi.org/10.3390/app7101064.

[18] M. Yanis, A.S. Mohruni, S. Sharif, I. Yani, Z. Suzen, Z.A. Ahmad, Cutting force prediction when green machining of thin-walled Ti-6Al-4V under dry and MQL-cutting using response surface methodology and artificial neural networks-algorithm, AIP Conf. Proc. 29 (1) (2019), 020027 (AIP Publishing LLC).

[19] S.O. Sada, S.C. Ikpeseni, Evaluation of ANN and ANFIS modelling ability in the prediction of AISI 1050 steel machining performance, Heliyon 7 (2) (2021), e06136, https://doi.org/10.1016/j.heliyon.2021.e06136.

[20] M.K. Gupta, M. Mia, C.I. Pruncu, A.M. Khan, M.A. Rahman, M. Jamil, V.S. Sharma, Modelling and performance evaluation of Al2O3, MoS2 and graphite nanoparticle-assisted MQL in turning titanium alloy: an intelligent approach, J. Braz. Soc. Mech. Sci. 42 (4) (2020) 1–21, https://doi.org/10.1007/s40430-020-2256-z.

[21] C.E. Onu, J.T. Nwabanne, P.E. Ohale, C.O. Asadu, Comparative analysis of RSM, ANN and ANFIS and the mechanistic modelling in eriochrome black-T dye adsorption using modified clay, South Afr. J. Chem. Eng. 36 (2021) 24–42, https://doi.org/10.1016/j.sajce.2020.12.003.

[22] V.S. Gadakh, Application of MOORA method for parametric optimization of milling process, Int. J. Appl. Eng. Res. 1 (4) (2010) 743.

[23] S. Kalirasu, N. Rajini, S. Rajesh, J.W. Jappes, K. Karuppasamy, AWJM Performance of jute/polyester composite using MOORA and analytical models, Mater. Manuf. Process. 32 (15) (2017) 1730–1739, https://doi.org/10.1080/10426914.2017.1279314.

[24] A. Khan, K. Maity, Parametric optimization of some non-conventional machining processes using MOORA method, Int. J. Eng. Res. Afr. 20 (2016) 19–40. https://dx.doi.org/10.4028/www.scientific.net/JERA.20.19.

[25] P. Karande, S. Chakraborty, Application of multi-objective optimization on the basis of ratio analysis (MOORA) method for materials selection, Mater. Des. 37 (2012) 317–324, https://doi.org/10.1016/j.matdes.2012.01.013.

[26] H. Majumder, K. Maity, Optimization of machining condition in WEDM for titanium grade 6 using MOORA coupled with PCA—a multivariate hybrid approach, J. Adv. Manuf. Syst. 16 (2) (2017) 81–99, https://doi.org/10.1142/S0219686717500068.

[27] P.B. Zaman, M.N. Sultana, N.R. Dhar, Multi-variant hybrid techniques coupled with Taguchi in multi-response parameter optimisation for better machinability of turning alloy steel, Adv Mater Process Technol 8 (3) (2021) 3127–3147, https://doi.org/10.1080/2374068X.2021.1945302.

[28] P. Li, H. Qian, J. Wu, J. Chen, Sensitivity analysis of TOPSIS method in water quality assessment: I. Sensitivity to the parameter weights, Environ. Monit. Assess. 185 (3) (2013) 2453–2461, https://doi.org/10.1007/s10661-012-2723-9.

[29] D. Bhadra, N.R. Dhar, M.A. Salam, Sensitivity analysis of the integrated AHP-TOPSIS and CRITIC-TOPSIS method for selection of the natural fiber, Mater. Today: Proc. 56 (2022) 2618–2629, https://doi.org/10.1016/j.matpr.2021.09.178.

[30] Y.C. Zhang, T. Mabrouki, D. Nelias, Y.D. Gong, Chip formation in orthogonal cutting considering interface limiting shear stress and damage evolution based on fracture energy approach, Fin elem anal des 47 (7) (2011) 850–863, https://doi.org/10.1016/j.finel.2011.02.016.

[31] M. Mia, N.R. Dhar, Response surface and neural network based predictive models of cutting temperature in hard turning, J. Adv. Res. 7 (6) (2016) 1035–1044, https://doi.org/10.1016/j.jare.2016.05.004.

[32] M. Ikhlas, Y.M. Athmane, B. Hamza, K. Ahmed, E. Mohamed, Prediction of surface roughness and cutting forces using RSM, ANN, and NSGA-II in finish turning of AISI 4140 hardened steel with mixed ceramic tool, Int. J. Adv. Manuf. Technol. 97 (5–8) (2018) 1931–1949, https://doi.org/10.1007/s00170-018-2026-6.

[33] P.B. Zaman, N.R. Dhar, Multi-objective optimization of double-jet MQL system parameters meant for enhancing the turning performance of Ti–6Al–4V alloy, Arabian J. Sci. Eng. 45 (11) (2020) 9505–9526, https://doi.org/10.1007/s13369-020-04806-x.

[34] M. Mia, M.A. Khan, N.R. Dhar, Study of surface roughness and cutting forces using ANN, RSM, and ANOVA in turning of Ti-6Al-4V under cryogenic jets applied at flank and rake faces of coated WC tool, Int. J. Adv. Manuf. Technol. 93 (1) (2017) 975–991, https://doi.org/10.1007/s00170-017-0566-9.

[35] C. Naresh, P.S. Bose, C.S. Rao, Artificial neural networks and adaptive neuro-fuzzy models for predicting WEDM machining responses of Nitinol alloy: comparative study, SN Appl. Sci. 2 (2) (2020) 1–23, https://doi.org/10.1007/s42452-020-2083-y.

[36] X.A. Vasanth, P.S. Paul, A.S. Varadarajan, A neural network model to predict surface roughness during turning of hardened SS410 steel, Int J Sys Assur Eng Manag 11 (3) (2020) 704–715, https://doi.org/10.1007/s13198-020-00986-9.

[37] M. Mia, N.R. Dhar, Prediction and optimization by using SVR, RSM and GA in hard turning of tempered AISI 1060 steel under effective cooling condition, Neural Comput. Appl. 31 (2019) 2349–2370, https://doi.org/10.1007/s00521-017-3192-4.

[38] I. Asilturk, M. Cunkas, Modelling and prediction of surface roughness in turning operations using artificial neural network and multiple regression method, Exp sys appl 38 (5) (2011) 5826–5832, https://doi.org/10.1016/j.eswa.2010.11.041.

[39] E. Ezugwu, D. Fadare, J. Bonney, R. Da Silva, W. Sales, Modelling the correlation between cutting and process parameters in high-speed machining of Inconel 718 alloy using an artificial neural network, Int. J. Mach. Tool Manufact. 45 (12) (2005) 1375–1385, https://doi.org/10.1016/j.ijmachtools.2005.02.004.

[40] J.S. Jang, Neuro-fuzzy modelling for dynamic system identification, in: Soft Computing in Intelligent Systems and Information Processing. Proceedings of the 1996 Asian Fuzzy Systems Symposium, IEEE, 1996, pp. 320–325, https://doi.org/10.1109/AFSS.1996.583623.

[41] S. Akbari, S.M. Mahmood, I.M. Tan, H. Hematpour, Comparison of neuro-fuzzy network and response surface methodology pertaining to the viscosity of polymer solutions, J. Pet. Explor. Prod. Technol. 8 (3) (2018) 887–900, https://doi.org/10.1007/s13202-017-0375-6.

[42] K. Pearson, On lines and planes of closest fit to systems of points in space, Philos Manag (1901) 559–572, https://doi.org/10.1080/14786440109462720.

[43] H. Hotelling, Analysis of a complex of statistical variables into principal components, J. Educ. Psychol. 24 (6) (1933) 417–441, https://doi.org/10.1037/h0071325.

[44] W.K. Brauers, E. Zavadskas, The MOORA method and its application to privatization in a transition economy, Control Cybern. 35 (2) (2006) 445–469.

[45] F. Pusavec, A. Deshpande, S. Yang, R. M'Saoubi, J. Kopac, O.W. Dillon Jr., I.S. Jawahir, Sustainable machining of high temperature Nickel alloy–Inconel 718: part 1–predictive performance models, J. Clean. Prod. 81 (2014) 255–269, https://doi.org/10.1016/j.jclepro.2014.06.040.
[46] G.R. Johnson, A constitutive model and data for materials subjected to large strains, high strain rates, and high temperatures, Proc. 7th Inf. Sympo. Ballistics (1983) 541–547.
[47] M. Mia, Multi-response optimization of end milling parameters under through-tool cryogenic cooling condition, Measurement 111 (2017) 134–145, https://doi.org/10.1016/j.measurement.2017.07.033.
[48] M.S. Hossain, N. Ahmad, Surface roughness prediction modelling for commercial dies using ANFIS, ANN and RSM, Int. J. Ind. Syst. Eng. 16 (2) (2014) 156–183, https://doi.org/10.1504/IJISE.2014.058834.